Published for SISSA by Springer

Received: October 2, 2013
Accepted: December 6, 2013
Published: January 9, 2014

A holographic p-wave superconductor model

Rong-Gen Cai,[a] **Li Li**[a] **and Li-Fang Li**[b]

[a] *State Key Laboratory of Theoretical Physics, Institute of Theoretical Physics, Chinese Academy of Sciences, Beijing 100190, China*

[b] *State Key Laboratory of Space Weather, Center for Space Science and Applied Research, Chinese Academy of Sciences, Beijing 100190, China*

E-mail: cairg@itp.ac.cn, liliphy@itp.ac.cn, lilf@itp.ac.cn

Abstract: We study a holographic p-wave superconductor model in a four dimensional Einstein-Maxwell-complex vector field theory with a negative cosmological constant. The complex vector field is charged under the Maxwell field. We solve the full coupled equations of motion of the system and find black hole solutions with the vector hair. The vector hairy black hole solutions are dual to a thermal state with the U(1) symmetry as well as the spatial rotational symmetry broken spontaneously. Depending on two parameters, the mass and charge of the vector field, we find a rich phase structure: zeroth order, first order and second order phase transitions can happen in this model. We also find "retrograde condensation" in which the hairy black hole solution exists only for the temperatures above a critical value with the free energy much larger than the one of the black hole without the vector hair. We construct the phase diagram for this system in terms of the temperature and charge of the vector field.

Keywords: Gauge-gravity correspondence, Holography and condensed matter physics (AdS/CMT)

ArXiv ePrint: 1309.4877

doi:10.1007/JHEP01(2014)032

JHEP01(2014)032

Contents

JHEP01(2014)032

1 Introduction

Due to the strong/weak duality characteristic of the Anti-de Sitter/Conformal Field Theory correspondence (AdS/CFT) [1–3], it provides us with a powerful approach to study the properties of strong coupled systems by a weak coupled AdS gravity. The high temperature superconductivity is a potential area where the AdS/CFT correspondence is applicable. According to the symmetry of the spatial part of wave function of the Cooper pair, superconductors can be classified as the s-wave, p-wave, d-wave, f-wave superconductor, etc. From a phenomenological perspective, the onset of superconductivity is characterized by the condensation of a composite charged operator spontaneously breaking U(1) symmetry at some temperature. The holographic s-wave superconductor model was first realized in refs. [4, 5]. According to the AdS/CFT correspondence, in the gravity side, a Maxwell field and a charged scalar field are introduced to describe the U(1) symmetry and the scalar operator in the dual field theory side. This holographic model undergoes a phase transition from black hole with no hair (normal phase/conductor phase) to the case with scalar hair at low temperatures (superconducting phase). Holographic d-wave model was constructed by introducing a charged massive spin two field propagating in the bulk [6–8]. To realize a holographic p-wave superconductor model, one needs to introduce a charged vector field in the bulk as a vector order parameter. Ref. [9] presented a holographic p-wave model by introducing a SU(2) Yang-Mills field into the bulk, where a gauge boson generated by one SU(2) generator is dual to the vector order parameter. Other generalized studies based on this model can be found for example in refs. [10–15]. An alternative holographic realization of p-wave superconductivity emerges from the condensation of a 2-form field in the bulk [16].

In a recent paper [17], we have studied a holographic model by introducing a complex vector field ρ_μ charged under a Maxwell gauge field A_μ in the bulk, which is dual to a strongly coupled system involving a charged vector operator with a global U(1) symmetry. In this model there exists a non-minimal coupling between the vector field and the gauge field characterizing the magnetic moment of the vector field, which plays a crucial role in the condensate of the vector field induced by an applied magnetic field. We have studied this model in the probe limit at finite density. Such a setup meets the minimum requirement to construct a holographic p-wave superconductor model. Indeed, we have found a critical temperature at which the system undergoes a second order phase transition. The critical exponent of this transition is one half which coincides with the case in the Landau-Ginzburg theory. In the condensed phase, a vector operator acquires a vacuum expectation value breaking the U(1) symmetry as well as rotational symmetry spontaneously. Our calculation indicates that this condensed phase exhibits an infinite DC conductivity and a gap in the optical conductivity, which is very reminiscent of some characteristics known from ordinary superconductivity. In this sense, our model can be regarded as a holographic p-wave model.

The probe approximation neglecting the back reaction of the matter fields is only justified in the limit of large q with $q\rho_\mu$ and qA_μ fixed. It has been shown that new phases can emerge (see refs. [18–20] for example) and the order of the phase transition can also be changed [21–25] once the back reaction of the matter fields on the geometry is taken into account. To study the complete phase diagram of our holographic system, we need to go beyond the probe approximation and to include the back reaction. While the previous paper [17] focused on the effects of the non-minimal coupling term and applied magnetic field on the condensate of the vector operator, in this paper we aim at studying the effect of the back reaction of the matter fields on the background geometry. We will turn off the non-minimal coupling between the vector field ρ_μ and the gauge field A_μ since we do not discuss magnetic effect in this paper. So the model is left with two independent parameters, i.e., the mass m of the vector field giving the dimension of the dual vector operator and its charge q controlling the strength of the back reaction on the background geometry. We manage to construct asymptotically AdS charged black hole solutions with nontrivial vector hair. It turns out that depending on m^2 and q, our model exhibits a rich phase structure.

The thermodynamic behavior of the model has a dramatic change from large m^2 to small m^2. In the case with large m^2, if one lowers the temperature, the normal phase will become unstable to developing vector hair below a critical temperature T_c. The transition from the normal phase to the condensed phase is second order for larger q, i.e., weak strength of the back reaction. However, as we decrease q to a critical one, the phase transition becomes first order. On the other hand, for the case with small m^2, no matter the value of q, there exists a temperature below which the condensed phase never exists. When the back reaction is weak, hairy solutions dominate the phase diagram below a critical temperature T_2 through a second order transition, then the condensed phase terminates at a lower temperature T_0 at which its free energy jumps to the one in the normal phase, indicating a zeroth order transition. As we strengthen the back reaction, we first encounter for a first order transition at temperature T_1 and then a zeroth order transition at T_0.

JHEP01(2014)032

For the sufficiently strong back reaction case, the condensed phase only occurs at a high temperature $T > T_n$ rather than at a low temperature. Furthermore, the hairy phase has higher free energy than the normal phase. The four critical transition temperatures T_c, T_2, T_1 and T_0 decrease as one increases the strength of the back reaction. To summarize possible phases associated with different ranges of model parameters, we construct the phase diagram in terms of charge q and temperature T for a given mass. We find that the critical temperature increases with the charge and decreases with the mass of ρ_μ.

This paper is organized as follows. In the next section, we introduce the holographic model and deduce the equations of motion of the model. In section 3, we give our ansatz for the hairy black hole solution corresponding to the condensed phase and specify the boundary conditions to be satisfied. Section 4 is devoted to calculating the free energy and dual stress-energy tensor. We present numerical results in section 5. For each given m^2, we scan a wide range of q to find all possible types of phase transitions and construct the phase diagram. The conclusion and some discussions are included in section 6.

2 The holographic model

Let us introduce a complex vector field ρ_μ, with mass m and charge q, into the $(3+1)$ dimensional Einstein-Maxwell theory with a negative cosmological constant. The complete action reads

$$\begin{aligned} S &= \frac{1}{2\kappa^2}\int d^4x\sqrt{-g}\left(\mathcal{R}+\frac{6}{L^2}+\mathcal{L}_m\right), \\ \mathcal{L}_m &= -\frac{1}{4}F_{\mu\nu}F^{\mu\nu}-\frac{1}{2}\rho^\dagger_{\mu\nu}\rho^{\mu\nu}-m^2\rho^\dagger_\mu\rho^\mu+iq\gamma\rho_\mu\rho^\dagger_\nu F^{\mu\nu}, \end{aligned} \tag{2.1}$$

with L the AdS radius set to be unity and $\kappa^2 \equiv 8\pi G$ related to the gravitational constant in the bulk. The Maxwell field strength reads $F_{\mu\nu} = \nabla_\mu A_\nu - \nabla_\nu A_\mu$. $\rho_{\mu\nu}$ in (2.1) is defined by $\rho_{\mu\nu} = D_\mu\rho_\nu - D_\nu\rho_\mu$ with the covariant derivative $D_\mu = \nabla_\mu - iqA_\mu$. The last non-minimal coupling term characterizes the magnetic moment of the vector field ρ_μ, which plays an important role in the case with an applied magnetic field [17]. In the present study, since we only consider the case without external magnetic field, this term will not play any role.

Varying the action (2.1), we obtain the equations of motion for matter fields

$$\nabla^\nu F_{\nu\mu} = iq(\rho^\nu\rho^\dagger_{\nu\mu}-\rho^{\nu\dagger}\rho_{\nu\mu})+iq\gamma\nabla^\nu(\rho_\nu\rho^\dagger_\mu-\rho^\dagger_\nu\rho_\mu), \tag{2.2}$$

$$D^\nu\rho_{\nu\mu}-m^2\rho_\mu+iq\gamma\rho^\nu F_{\nu\mu} = 0, \tag{2.3}$$

and the equations of gravitational field

$$\begin{aligned} \mathcal{R}_{\mu\nu}-\frac{1}{2}\mathcal{R}g_{\mu\nu}-\frac{3}{L^2}g_{\mu\nu} &= \frac{1}{2}F_{\mu\lambda}F_\nu{}^\lambda+\frac{1}{2}\mathcal{L}_m g_{\mu\nu} \\ &\quad+\frac{1}{2}\left\{\left[\rho^\dagger_{\mu\lambda}\rho_\nu{}^\lambda+m^2\rho_\mu{}^\dagger\rho_\nu-iq\gamma(\rho_\mu\rho_\lambda{}^\dagger-\rho_\mu{}^\dagger\rho_\lambda)F_\nu{}^\lambda\right]+\mu\leftrightarrow\nu\right\}. \end{aligned} \tag{2.4}$$

In the AdS/CFT correspondence, a hairy black hole with appropriate boundary conditions can be explained as a condensed phase of the dual field theory, while a black hole

JHEP01(2014)032

without hair is dual to an uncondensed phase (normal phase). In our case, since ρ_μ is charged under the U(1) gauge field, its dual operator will carry the same charge under this gauge symmetry and a vacuum expectation value of this operator will then trigger the U(1) symmetry breaking spontaneously. More precisely, we hope that this system would admit hairy black hole solutions at low temperatures, but no hair at high temperatures. Thus, the condensate of the dual vector operator will break the U(1) symmetry as well as the spatial rotational symmetry since the condensate will pick out one direction as special. Therefore, viewing this vector field as an order parameter, the holographic model can be used to mimic a p-wave superconductor (superfluid) phase transition. This turns out to be true in the probe limit [17]: when one lowers the temperature to a certain value, the normal background becomes unstable and a nontrivial vector hair ρ_x appears. In this paper, we continue to study this model by considering the back reaction of matter fields on the background geometry.

3 Equations of motion and boundary conditions

To construct homogeneous charged black hole solutions with vector hair, we adopt the following ansatz

$$\begin{aligned} ds^2 &= -f(r)e^{-\chi(r)}dt^2 + \frac{dr^2}{f(r)} + r^2h(r)dx^2 + r^2dy^2, \\ \rho_\nu dx^\nu &= \rho_x(r)dx\,, \qquad A_\nu dx^\nu = \phi(r)dt\,. \end{aligned} \tag{3.1}$$

We will denote the position of the horizon as r_h and the conformal boundary will be at $r \to \infty$. Our consideration is as follows. Since we would like to study a dual theory with finite chemical potential or charge density accompanied by a U(1) symmetry, we turn on A_t in the bulk. We want to allow for states with a non-trivial current $\langle \hat{J}_x \rangle$, for which we further introduce ρ_x in the bulk. Because a non-vanishing $\langle \hat{J}_x \rangle$ picks out x direction as special, which obviously breaks the rotational symmetry in $x-y$ plane. Therefore we introduce a function $h(r)$ in the xx component of the metric in order to describe the anisotropy.

The horizon r_h is determined by $f(r_h) = 0$. The temperature T of the black hole is given by

$$T = \frac{f'(r_h)e^{-\chi(r_h)/2}}{4\pi}\,, \tag{3.2}$$

and the thermal entropy S is given by the Bekenstein-Hawking entropy of the black hole

$$S = \frac{2\pi}{\kappa^2}A = \frac{2\pi V_2}{\kappa^2}r_h^2\sqrt{h(r_h)}\,, \tag{3.3}$$

where A denotes the area of the horizon and $V_2 = \int dxdy$.

One finds that the r component of (2.2) implies that the phase of ρ_x must be constant. Without loss of generality, we can take ρ_x to be real. Then, the independent equations of

JHEP01(2014)032

motion in terms of the above ansatz are deduced as follows

$$\begin{aligned}
\phi'' + \left(\frac{h'}{2h} + \frac{\chi'}{2} + \frac{2}{r}\right)\phi' - \frac{2q^2\rho_x^2}{r^2 f h}\phi = 0\,,\\
\rho_x'' + \left(\frac{f'}{f} - \frac{h'}{2h} - \frac{\chi'}{2}\right)\rho_x' + \frac{e^{\chi}q^2\phi^2}{f^2}\rho_x - \frac{m^2}{f}\rho_x = 0\,,\\
\chi' - \frac{2f'}{f} - \frac{h'}{h} + \frac{\rho_x'^2}{rh} - \frac{re^{\chi}\phi'^2}{2f} - \frac{e^{\chi}q^2\rho_x^2\phi^2}{rf^2h} + \frac{6r}{L^2 f} - \frac{2}{r} = 0\,,\\
h'' + \left(\frac{f'}{f} - \frac{h'}{2h} - \frac{\chi'}{2} + \frac{2}{r}\right)h' + \frac{2\rho_x'^{\,2}}{r^2} - \frac{2e^{\chi}q^2\rho_x^2\phi^2}{r^2 f^2} + \frac{2m^2\rho_x^2}{r^2 f} = 0\,,\\
\left(\frac{2}{r} - \frac{h'}{2h}\right)\frac{f'}{f} + \left(\frac{1}{r} + \frac{\chi'}{2}\right)\frac{h'}{h} - \frac{\rho_x'^2}{r^2 h} + \frac{e^{\chi}\phi'^2}{2f} + \frac{3e^{\chi}q^2\rho_x^2\phi^2}{r^2 f^2 h} - \frac{m^2\rho_x^2}{r^2 f h} - \frac{6}{L^2 f} + \frac{2}{r^2} = 0\,,
\end{aligned} \tag{3.4}$$

where the prime denotes the derivative with respect to r.

The full coupled equations of motion do not admit an analytical solution with non-trivial ρ_x. Therefore, we have to solve them numerically. We will use shooting method to solve equations (3.4). In order to find the solutions for all the five functions $\mathcal{F} = \{\rho_x, \phi, f, h, \chi\}$ one must impose suitable boundary conditions at both conformal boundary $r \to \infty$ and the horizon $r = r_h$.

In order to match the asymptotical AdS boundary, the general falloff near the boundary $r \to \infty$ behaves as

$$\begin{aligned}
&\phi = \mu - \frac{\rho}{r} + \dots\,, && \rho_x = \frac{\rho_{x-}}{r^{\Delta_-}} + \frac{\rho_{x+}}{r^{\Delta_+}} + \dots\,,\\
&f = r^2\left(1 + \frac{f_3}{r^3}\right) + \dots\,, && h = 1 + \frac{h_3}{r^3} + \dots\,, \qquad \chi = 0 + \frac{\chi_3}{r^3} + \dots\,,
\end{aligned} \tag{3.5}$$

where the dots stand for the higher order terms in the expansion in power of $1/r$ and $\Delta_\pm = \frac{1\pm\sqrt{1+4m^2}}{2}$.[1] We impose $\rho_{x-} = 0$ since we want the condensate to arise spontaneously. According to the AdS/CFT dictionary, up to a normalization, the coefficients μ, ρ, ρ_{x+} are regarded as chemical potential, charge density and the x component of the vacuum expectation of the vector operator $\hat{J}^\mu$ in the dual field theory, respectively.

We are interested in black hole configurations that have a regular event horizon located at r_h. Therefore, in addition to $f(r_h) = 0$, one must require $\phi(r_h) = 0$ in order for $g^{\mu\nu}A_\mu A_\nu$ being finite at the horizon. We require the regularity conditions at the horizon $r = r_h$, which means that all our functions have finite values and admit a series expansion in terms of $(r - r_h)$ as

$$\mathcal{F} = \mathcal{F}(r_h) + \mathcal{F}'(r_h)(r - r_h) + \cdots\,. \tag{3.6}$$

By plugging the expansion (3.6) into (3.4), one can find that there are five independent parameters at the horizon $\{r_h, \rho_x(r_h), \phi'(r_h), h(r_h), \chi(r_h)\}$. However, there are three useful

[1] The m^2 has a lower bound as $m^2 = -1/4$ with $\Delta_+ = \Delta_- = 1/2$. In that case, there is a logarithmic term in the asymptotical expansion. We treat such a term as the source set to be zero to avoid the instability induced by this term [26]. The treatment for $m^2 = -1/4$ is very subtle. We will not discuss this case in this paper and instead we are going to give a detailed study in future.

JHEP01(2014)032

scaling symmetries in the equations of motion, which read

$$e^{\chi} \to \lambda^2 e^{\chi}, \qquad t \to \lambda t\,, \qquad \phi \to \lambda^{-1}\phi\,, \tag{3.7}$$

$$\rho_x \to \lambda \rho_x\,, \qquad x \to \lambda^{-1} x\,, \qquad h \to \lambda^2 h\,, \tag{3.8}$$

and

$$r \to \lambda r\,, \qquad (t,x,y) \to \lambda^{-1}(t,x,y)\,, \qquad (\phi,\rho_x) \to \lambda(\phi,\rho_x)\,, \qquad f \to \lambda^2 f\,, \tag{3.9}$$

where in each case λ is a real positive number.

Taking advantage of above three scaling symmetries, we can first set $\{r_h = 1, \chi(r_h) = 0, h(r_h) = 1\}$ for performing numerics. After solving the coupled differential equations, we should use the first two symmetries again to satisfy the asymptotic conditions $\chi(\infty) = 0$ and $h(\infty) = 1$. Thus we finally have two independent parameters $\{\rho_x(r_h), \phi'(r_h)\}$ at hand. We shall use $\phi'(r_h)$ as the shooting parameter to match the source free condition, i.e., $\rho_{x-} = 0$. After solving the set of equations, we can obtain the condensate $\langle \hat{J}^x \rangle$, chemical potential μ and charge density ρ by reading off the corresponding coefficients in (3.5), respectively.

Under the third symmetry, the revelent quantities transform as

$$T \to \lambda T\,, \qquad S \to S\,, \qquad \mu \to \lambda \mu\,, \qquad \rho \to \lambda^2 \rho\,, \qquad \rho_{x+} \to \lambda^{\Delta_+ + 1} \rho_{x+}\,. \tag{3.10}$$

We will use the transformation to fix the chemical potential for each solution the same, i.e., we work in grand canonical ensemble.

Note that the set of equations admits an analytical solution with vanishing ρ_μ, corresponding to the normal phase (conductor phase). This solution is just the AdS Reissner-Nordström black hole, given by

$$\begin{aligned} ds^2 &= -f(r)dt^2 + \frac{dr^2}{f(r)} + r^2(dx^2 + dy^2)\,, \\ f(r) &= r^2 - \frac{1}{r}\left(r_h^3 + \frac{\mu^2 r_h}{4}\right) + \frac{\mu^2 r_h^2}{4r^2}\,, \qquad \phi(r) = \mu\left(1 - \frac{r_h}{r}\right), \end{aligned} \tag{3.11}$$

with the temperature $T = \frac{r_h}{4\pi}\left(3 - \frac{\mu^2}{4r_h^2}\right)$ and the entropy $S = \frac{2\pi V_2}{\kappa^2} r_h^2$.

4 Free energy and dual stress-energy tensor

In order to determine which phase is thermodynamically favored, we should calculate the free energy of the system for both normal phase and condensed phase. We will work in grand canonical ensemble in this paper, where the chemical potential is fixed. In gauge/gravity duality the grand potential Ω of the boundary thermal state is identified with temperature T times the on-shell bulk action in Euclidean signature. The Euclidean action must include the Gibbons-Hawking boundary term for a well-defined Dirichlet variational principle and further a surface counterterm for removing divergence. Since we consider a stationary problem, the Euclidean action is related to the Minkowski one by a minus sign as

$$-2\kappa^2 S_{\text{Euclidean}} = \int dx^4 \sqrt{-g}\,(\mathcal{R} + 6 + \mathcal{L}_m) + \int_{r\to\infty} d^3x \sqrt{-\bar{h}}\,(2\mathcal{K} - 4)\,, \tag{4.1}$$

JHEP01(2014)032

where $\bar{h}$ is the determinant of the induced metric $\bar{h}_{\mu\nu}$ on the boundary, and $\mathcal{K}$ is the trace of the extrinsic curvature $\mathcal{K}_{\mu\nu}$.[2]

Employing the equations of motion, the on-shell action reduces to

$$-2\kappa^2 S_{\text{Euclidean}}^{\text{on-shell}} = 2\beta V_2 e^{-\chi/2} r\sqrt{fh}\,(\mathcal{K}r - 2r - \sqrt{f})|_{r\to\infty}\,, \tag{4.2}$$

with $\beta = 1/T$ and $V_2 = \int dxdy$. Substituting the asymptotical expansion (3.5) into (4.1), we obtain

$$\Omega = TS_{\text{Euclidean}}^{\text{on-shell}} = \frac{V_2}{2\kappa^2} f_3\,, \tag{4.3}$$

where we have used the condition $h_3 = \chi_3$ which can be easily found form the equations of motion (3.4). Note that for the normal phase shown in (3.11), one has $f_3 = -r_h^3 - \frac{\mu^2 r_h}{4}$, and $h_3 = \chi_3 = 0$.

According to the AdS/CFT dictionary, the stress-energy tensor of the dual field theory can be calculated by [27]

$$T_{ij} = \frac{1}{\kappa^2}\lim_{r\to\infty}\left[r(\mathcal{K}\bar{h}_{ij} - \mathcal{K}_{ij} - 2\bar{h}_{ij})\right], \tag{4.4}$$

with $i, j = \{t, x, y\}$. By using of the asymptotical expansion (3.5), we have

$$\begin{aligned} T_{tt} &= \frac{1}{2\kappa^2}(-2f_3 + 3h_3)\,,\\ T_{xx} &= \frac{1}{2\kappa^2}(-f_3 + 3h_3)\,,\\ T_{yy} &= \frac{1}{2\kappa^2}(-f_3)\,, \end{aligned} \tag{4.5}$$

with vanishing non-diagonal components. For the normal phase with $h_3 = \chi_3 = 0$, we find that $T_{xx} = T_{yy}$ and $\Omega/V_2 = -T_{yy}$; the former shows the isotropy in $x - y$ plane and the latter gives the correct thermodynamical relation for the dual field theory to the AdS Reissner-Nordström black hole. In the condensed phase with nonzero $\langle \hat{J}_x \rangle$, the rotational symmetry is broken, thus it is expected to have $T_{xx} \neq T_{yy}$. But in both cases, the stress energy tensor is traceless, which is consistent with the fact that we are considering a dual conformal field theory at the AdS boundary.

5 Phase transition

In what follows we will look for condensed phases numerically. We take different m^2's into consideration and for each m^2 we scan a wide range of q which determines the strength of the back reaction of matter fields on the background. Our numerical results reveal that the system exhibits distinguished behavior depending on concrete value of m^2. There exists a particular value of m^2, for which we denote as m_c^2. In the case with $m^2 > m_c^2$, the condensed phase seems to survive even down to sufficiently low temperatures, i.e., $T \to 0$. In contrast, in the case with $m^2 < m_c^2$, the condensed phase cannot exist below

[2] In principle, we should also consider the surface counterterm for the charged vector field ρ_μ, but one can easily see that this term makes no contribution under the source free condition, i.e., $\rho_{x-} = 0$.

JHEP01(2014)032

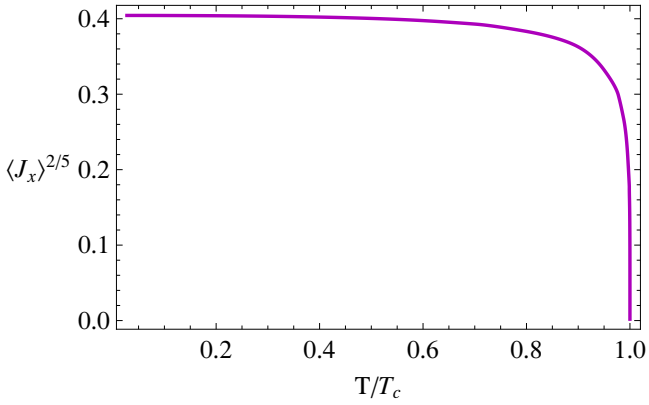

Figure 1. The condensate $\langle \hat{J}_x \rangle$ as a function of temperature. We choose $q = 1.5$ and $m^2 = 3/4$. The condensate begins to appear at $T_c \simeq 0.0179\mu$ and rises continuously as one further lowers the temperature, signaling a second order transition.

a finite temperature. To determine the precise value for m_c^2, we need to solve the coupled equations of motion (3.4) at very low temperatures to see whether the condensate would turn back to a higher temperature. The $T \to 0$ limit is a challenge in numerical calculation. Nevertheless, our numerical calculation suggests that $m_c^2 = 0$, for which we have some to say below. We will consider one concrete example for both cases. In each case we find similar results for other values of m^2.

5.1 $m^2 = 3/4$

For the case with $m^2 > m_c^2$, we choose $m^2 = 3/4$ as a concrete example. For each value of q, the AdS Reissner-Nordström solution always exists even down to the zero temperature limit. However, for sufficiently low temperature, we always find additional solutions with non-vanishing ρ_x that are thermodynamically preferred. That is to say, for each value of q we take, there is a phase transition occurring at a certain temperature T_c, where a charged black hole developing vector hair becomes thermodynamically favored. In the dual field theory side, it means that a vector operator acquires a vacuum expectation value $\langle \hat{J}_x \rangle \neq 0$ breaking the U(1) symmetry spontaneously. Furthermore, the condensate $\langle \hat{J}_x \rangle$ chooses a special direction, so the rotational symmetry in $x-y$ plane is also destroyed. Our numerical calculation indicates that the order of the phase transition can be changed from second order to first order as one increases the strength of the back reaction. More precisely, the phase transition is second order for $q > q_c$ and first order for $q < q_c$, where $q_c \simeq 1.3575$ for $m^2 = 3/4$.

Taking $q = 1.5 > q_c$ as a typical example, apart from the AdS Reissner-Nordström solution, we find another set of solutions with nonzero $\langle \hat{J}_x \rangle$ appearing below the critical temperature T_c. Figure 1 presents the condensate as a function of temperature, from which one can see that $\langle \hat{J}_x \rangle$ rises continuously from zero at T_c. The grand potential Ω is drawn in the left plot of figure 2. It is clear that below the critical temperature T_c, the state with non-vanishing vector "hair" is indeed thermodynamically favored over the normal phase. We draw the thermal entropy S with respect to temperature in the right plot of

JHEP01(2014)032

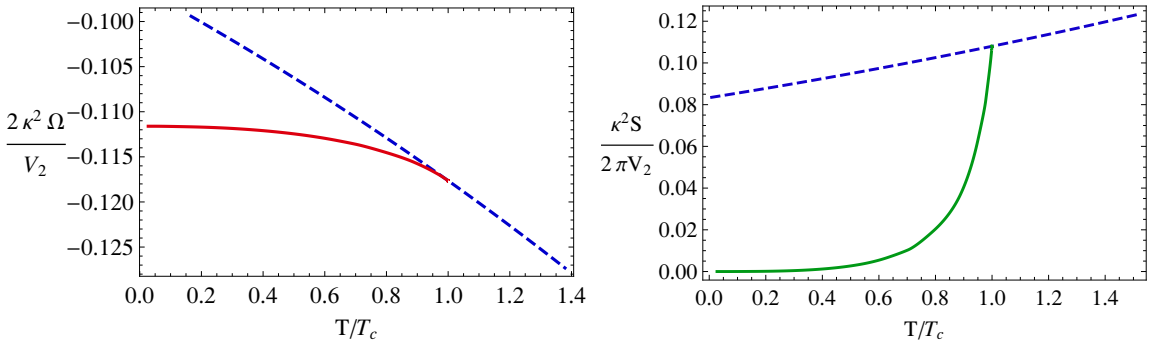

Figure 2. The grand potential Ω (left plot) and thermal entropy S (right plot) as a function of temperature. In both plots, the dashed blue curves are for the normal phase, while the solid curves are for the condensed phase. For $T > T_c$, one can only get the blue curve, but for lower temperature $T < T_c$ the condensed phase appears and has the lower free energy, thus is thermodynamically favored.

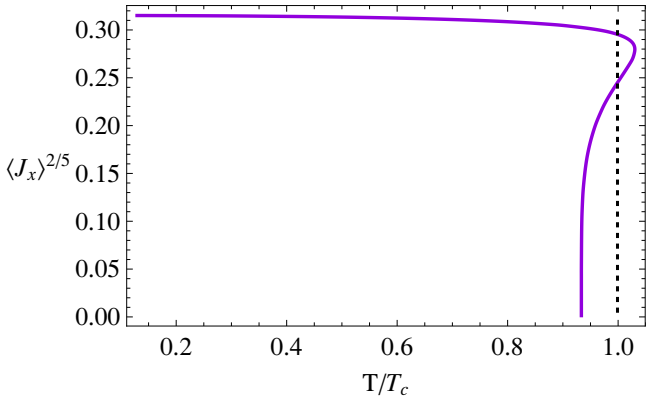

Figure 3. The condensate $\langle\hat{J}_x\rangle$ as a function of temperature for $q = 1.2$ and $m^2 = 3/4$. The critical temperature $T_c \simeq 0.00342\mu$ is denoted by a vertical dotted line. The condensate becomes multi-valued at $T \simeq 1.03T_c$. The value of condensate has a sudden jump from zero to the upper part of the purple solid curve at T_c, indicating a first order transition.

figure 2. One can see that at the critical temperature T_c, the entropy S is continuous but its derivative has a jump, indicating a second order phase transition. Our numerical results also suggest that the critical exponent for all $q > q_c$ is always 1/2, i.e., $\langle\hat{J}_x\rangle \sim (1-T/T_c)^{1/2}$.

A qualitative change happens as we decrease q past q_c. Consider the case with $q = 1.2 < q_c$. The condensate $\langle\hat{J}_x\rangle$ versus temperature is presented in figure 3. Compared to the previous case, the condensate becomes multi-valued and we can find two new sets of solutions with non-vanishing $\langle\hat{J}_x\rangle$ at temperatures lower than $T \simeq 1.03T_c$, involving an upper-branch with large $\langle\hat{J}_x\rangle$ and a down-branch with small $\langle\hat{J}_x\rangle$. Therefore, there are three states that are available to the system at some temperature, i.e., one is for $\langle\hat{J}_x\rangle = 0$ and two for $\langle\hat{J}_x\rangle \neq 0$. To determine which is the physical state, we draw the grand potential Ω in figure 4. One can find that the free energy versus temperature develops a characteristic "swallow tail" which is typical in first order phase transition. The normal phase is thermodynamically favored at higher temperatures, but as we lower

JHEP01(2014)032

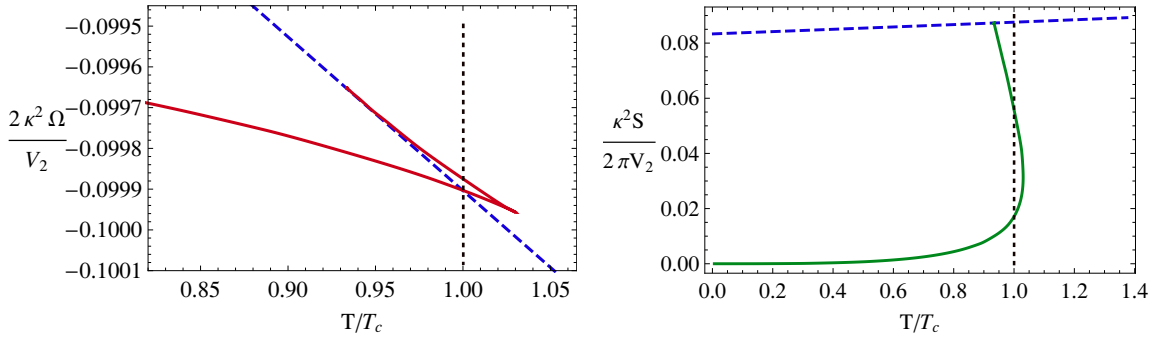

Figure 4. The grand potential Ω (left plot) and thermal entropy S (right plot) with respect to temperature with $q = 1.2$ and $m^2 = 3/4$. In both plots, dashed blue curves come from the normal phase, while the solid curves come from the condensed phase. Trace the physical curve by choosing the lowest grand potential at a fixed T. The critical temperature at which the condensed phase begins to be thermodynamically favored is $T_c \simeq 0.00342\mu$, denoted by a vertical dotted line. The entropy jumps from the blue curve to the lowest branch of the green solid curve at T_c.

the temperature down to T_c, the upper-branch finally dominates the system. We present the entropy S versus temperature in the right part of figure 4, from which one can see that S is also multi-valued and has a sudden jump from the normal phase to the physical condensed phase at T_c. Clearly, the transition is first order.

One interesting feature presented in both cases is that the hairy black hole exhibits tiny entropy at finite low temperatures, compared with the normal phase in figure 2 and figure 4. Since the values of S are obtained from the behavior of the solutions at the horizon, it is difficult to extract them with high accuracy at sufficiently low temperature. Nevertheless, our numerical results suggest that entropy remains small and smoothly decreases as the temperature is gradually lowered. As being a single state without any degeneracy, a superconducting ground state should not have any entropy. In the gravity side, it corresponds to the fact that the zero temperature limit of the superconducting black holes should have zero horizon area, which was previously observed in refs. [28, 29].

The main results of this subsection are summarized by the (T, q) phase diagram shown in figure 5. The solid curve gives the critical temperature T_c for the phase transition from the normal phase to the condensed phase. There is a critical value of q, denoted as q_c, above which the phase transition is second order, while below which the transition becomes first order. It is also clearly that as q decreases, T_c decreases gradually, which tells us that the increase of the back reaction hinders the phase transition.

5.2 $m^2 = -3/16$

Similar to the previous discussion, for each $m^2 < m_c^2$ we scan a wide range of q to find all possible types of transitions. There exist two special values of q, denoted as q_α and q_β with $q_\alpha > q_\beta$, which divides the parameter space of q into three regions, $q > q_\alpha$, $q_\beta < q < q_\alpha$ and $q < q_\beta$, respectively. The thermodynamic behavior changes qualitatively in three regions. We may find second order transition, first order transition and zeroth order transition. In order to take account of the order of the phase transitions, we denote the transition

JHEP01(2014)032

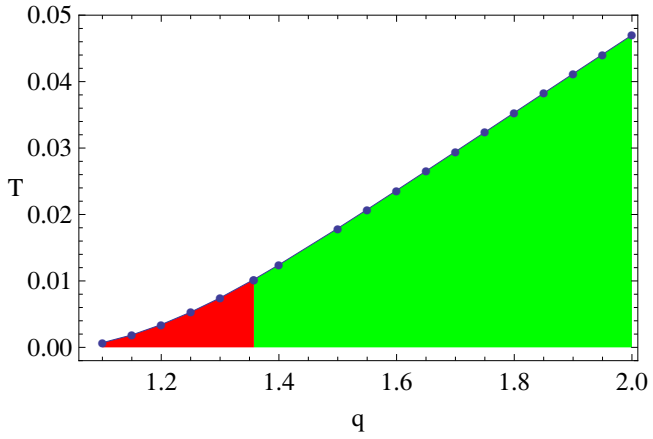

Figure 5. The phase diagram for $m^2 = 3/4$. The solid curve separates the condensed phase from the normal phase. The critical value q_c divides the condensed phase into two parts. The case $q > q_c$ is associated with second order phase transition (green area), while $q < q_c$ corresponds to first order transition (red area).

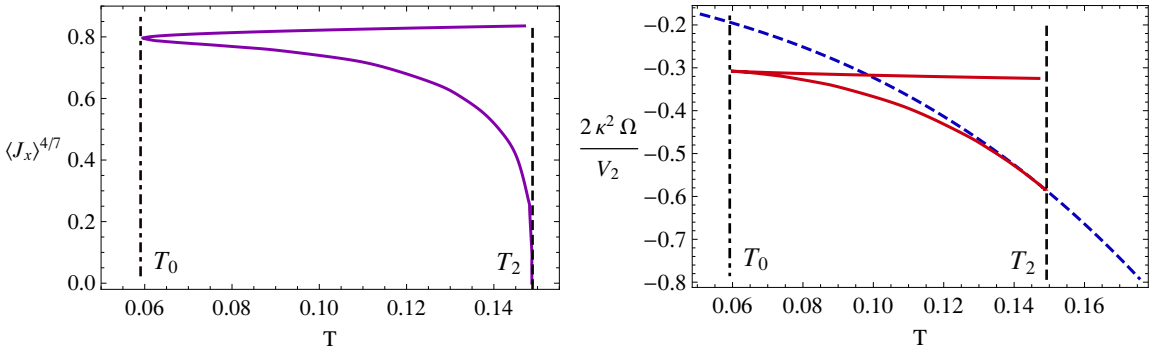

Figure 6. The condensate $\langle \hat{J}_x \rangle$ (left) and free energy Ω (right) as a function of temperature for $q = 2$ and $m^2 = -3/16$. The dashed blue curve is from the normal phase, while the solid curves are from the condensed phase. $T_2 \simeq 0.1487\mu$ is denoted by a vertical dashed line and $T_0 \simeq 0.05972\mu$ is denoted by a vertical dot dashed line. The condensate becomes multi-valued between T_0 and T_2. The lower branch of the condensed phase has the lowest free energy. For temperatures $T < T_0$ and $T > T_2$, the normal phase is thermodynamically preferred.

temperature as T_2, T_1 and T_0, respectively. As a typical example, we will take the mass parameter $m^2 = -3/16$ in this subsection. In this case $q_\alpha \simeq 1.0175$ and $q_\beta \simeq 0.9537$. Details are given as follows.

For the case with small back reaction, i.e., $q > q_\alpha$, we focus on the case with $q = 2$. The condensate versus temperature is exhibited in the left plot of figure 6. We immediately see that $\langle \hat{J}_x \rangle$ is multi-valued above the temperature denoted as $T_0 \simeq 0.05972\mu$. Similar to the first order transition for $m^2 = 3/4$, the condensed phase has two branches, i.e., the upper-branch with large $\langle \hat{J}_x \rangle$ and a down-branch with small $\langle \hat{J}_x \rangle$. The free energy Ω drawn in the right plot of figure 6 also shows a "swallow tail" shape, but it is very different from the one in figure 4. Comparing the free energy Ω for each solution, we find

JHEP01(2014)032

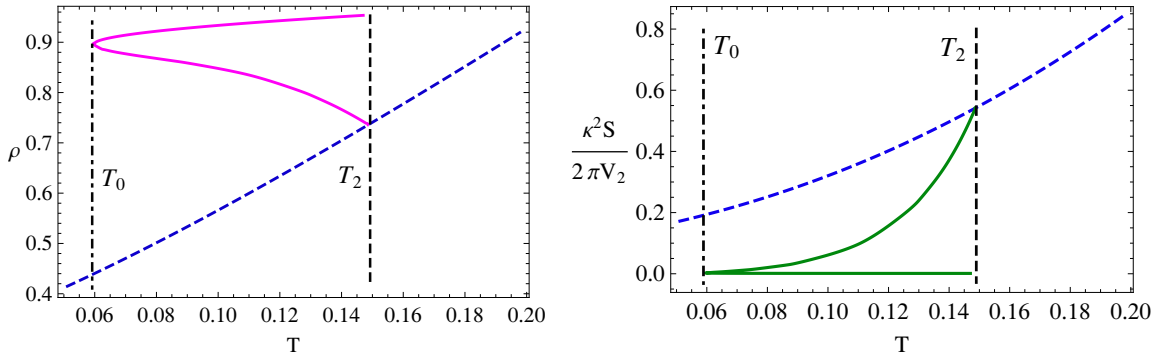

Figure 7. The charge density ρ (left) and thermal entropy S (right) versus temperature for $q = 2$ and $m^2 = -3/16$. The dashed blue curves are for the normal phase, while the solid curves for the condensed phase. $T_2 \simeq 0.1487\mu$ is denoted by a vertical dashed line and $T_0 \simeq 0.0597\mu$ is denoted by a vertical dot dashed line. As $T_0 < T < T_2$, ρ and S become multi-valued between, where only the lower branch of the charge density and the upper branch of the entropy are thermodynamically preferred. In other region of temperature, the normal phase dominates the phase diagram. Both ρ and S are continuous but not differentiable at T_2, characterizing a second order phase transition.

that the condensed solutions in the down-branch are thermodynamically favored, which only exist in a small range $T_0 < T < T_2$. At other temperatures, including $T < T_0$ and $T > T_2$, it is the normal phase with $\langle \hat{J}_x \rangle = 0$ that is thermodynamically relevant. At the temperature T_0, the free energy has a sudden jump from the condensed phase to the normal phase, indicating a zeroth order transition. The charge density ρ and entropy S in figure 7 show that both ρ and S are continuous but have a kink at T_2, indicating a second order transition. It is interesting to note that the condensed phase terminates at a finite lower temperature T_0.

For the case $q_\beta < q < q_\alpha$, let us consider for example the case with $q = 39/40$. The behaviors of condensate and other thermodynamical quantities are much more complicated. Figure 8 plots the condensate with respect to temperature, where $\langle \hat{J}_x \rangle$ is also multi-valued above $T_0 \simeq 0.03992\mu$. But there are three sets of condensed solutions. According to the value of condensate, we denote them as the upper-branch for large $\langle \hat{J}_x \rangle$, the middle-branch for middle $\langle \hat{J}_x \rangle$ and the down-branch for small $\langle \hat{J}_x \rangle$, respectively. We also draw the grand potential Ω in the right plot of figure 8. We present the charge density as well as the thermal entropy in figure 9. The values of ρ and S have a sudden jump from the normal phase to the thermodynamically favored branch of the condensed phase at T_1, indicating a first order phase transition. As we lower the temperature, the phase with $\langle \hat{J}_x \rangle = 0$ is first thermodynamically favored, and then the middle-branch begins to dominate the thermodynamics through a first order transition at $T_1 \simeq 0.04102\mu$, finally the condensed phase ends up at the temperature T_0 where a zeroth order transition appears. Our numerical results uncover that as one increases the strength of the back reaction, T_1 decreases while T_0 also decrease but with a slowly rate, and finally T_1 becomes equal to T_0 at q_β. For the present case $q_\beta < q < q_\alpha$, the value of T_1 is always larger than T_0, so we have a first order transition from the normal phase to the condensed phase at higher

JHEP01(2014)032

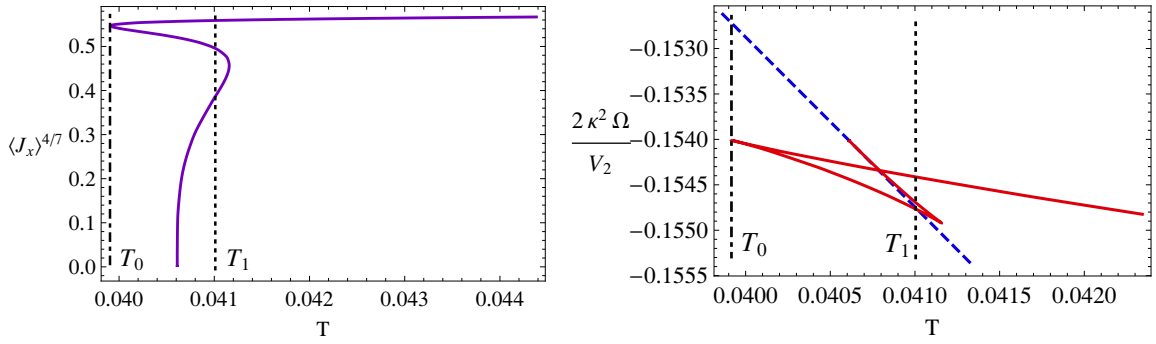

Figure 8. The condensate $\langle \hat{J}_x \rangle$ (left) and free energy Ω (right) as a function of temperature for $q = 39/40$ and $m^2 = -3/16$. The dashed blue curve is from the normal phase, while the solid curves are from the condensed phase. $T_1 \simeq 0.04102\mu$ is denoted as a vertical dashed line and $T_0 \simeq 0.03992\mu$ is denoted as a vertical dot dashed line. The condensate behaves multi-valued. The middle branch of the condensed phase has the lowest free energy between T_0 and T_1. For other range of temperature, the normal phase is thermodynamically favored.

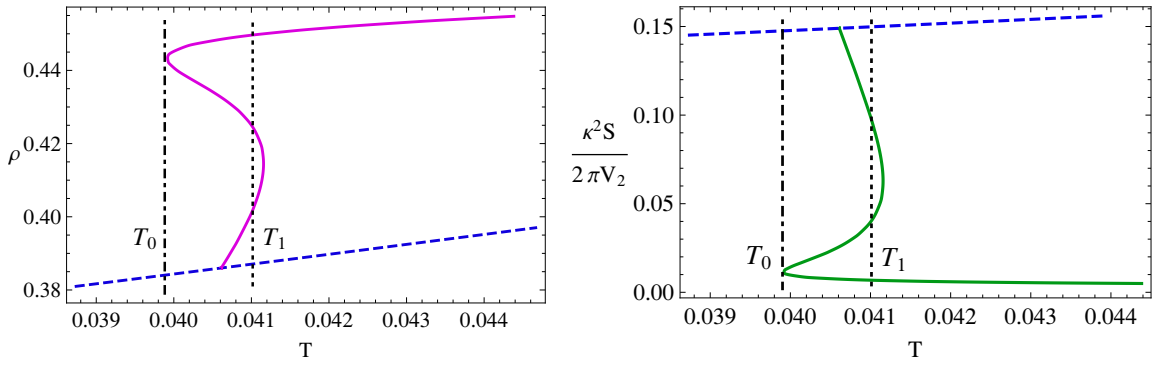

Figure 9. The charge density ρ (left) and thermal entropy S (right) versus temperature for $q = 39/40$ and $m^2 = -3/16$. The dashed blue curves correspond to the normal phase, while the solid curves to the condensed phase. $T_1 \simeq 0.04102\mu$ is denoted by a vertical dotted line and $T_0 \simeq 0.03992\mu$ is denoted by a vertical dot dashed line. When $T_0 < T < T_1$, ρ and S are both multi-valued. In both plots, it is the middle branch that is thermodynamically preferred. In other region of temperature, the normal phase is thermodynamically favored. Both ρ and S are not continuous at T_1, but rather jump from the blue dashed line to the middle branch of the solid line, signaling a first order transition.

temperature T_1 and then a zeroth order transition from the condensed phase to the normal phase at lower temperature T_0.

For the above two examples, an interesting common feature is that the thermodynamically favored hairy black hole solutions exist up to a minimal temperature T_0, where it connects with an unstable condensed branch starting from higher temperature, which will be discussed below. In the present model we restrict the case with ρ_x turned on, only the uncondensed phase can appear below T_0, so the free energy has a sudden jump from the condensed phase to the normal phase at T_0, indicating a zeroth order transition. Note that in the theory of superfluidity and superconductivity, a discontinuity of the free energy was

JHEP01(2014)032

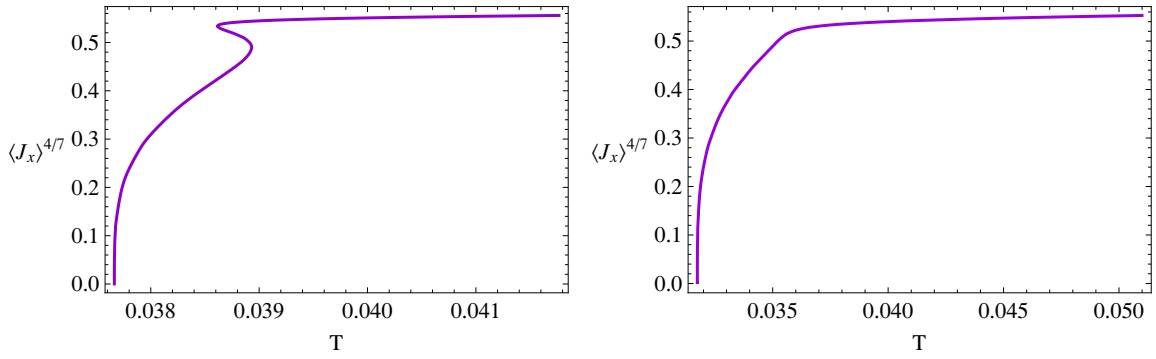

Figure 10. The condensate $\langle \hat{J}_x \rangle$ as a function of temperature for $q = 19/20$ (left) and $q = 9/10$ (right). The condensate only emerges above the temperature $T_n \simeq 0.03766\mu$ for $q = 19/20$ and $T_n \simeq 0.03174\mu$ for $q = 9/10$. The condensate in the left plot behaves multi-valued.

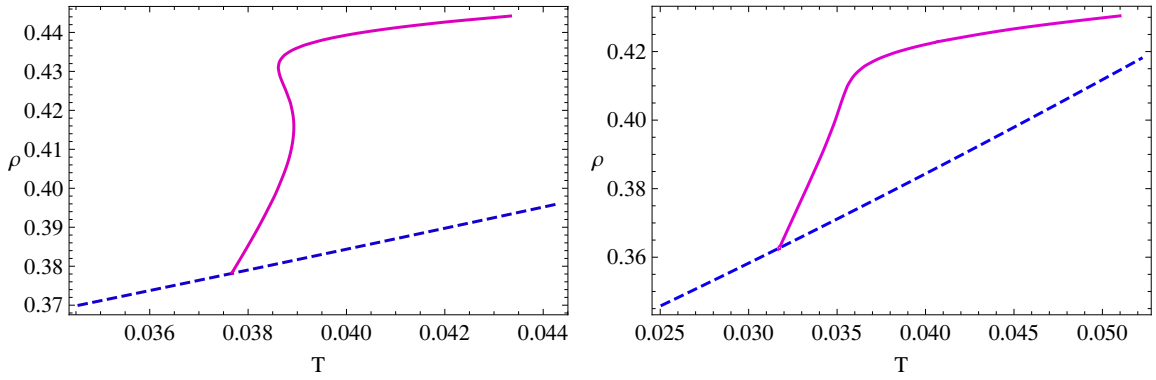

Figure 11. The charge density ρ as a function of temperature for $q = 19/20$ (left) and $q = 9/10$ (right). The dashed blue curves come from the normal phase, while the solid curves from the condensed phase.

discovered theoretically and an exactly solvable model for such phase transition was given in ref. [30]. Therefore, it is quite interesting to see whether the holographic model has some relation to the model in ref. [30].

As q decreases past q_β, we see a dramatic change in the thermodynamics. We draw the condensate versus temperature in figure 10 for $q = 19/20$ and $q = 9/10$, from which we can find that hairy solutions only appear at temperatures above T_n and the general trend is that $\langle \hat{J}_x \rangle$ increases with the temperature.[3] The value of $\langle \hat{J}_x \rangle$ is multi-valued for the case with larger q. As we decrease q, this multi valuedness disappears. For completeness, we show the charged density ρ in figure 11 and the thermal entropy S in figure 12. Similar feature can also be found in these two figures. At a first glance, this appears to be surprising, since in general one expects the condensed phase to emerge at low temperatures rather than at high temperatures. To have a physical condensed phase, the hairy black hole

[3]One may wonder if the curve could turn back at a higher temperature. We numerically check this increasing trend up to a very high temperature as we can and find the curve has a well defined asymptotic behavior. Therefore, we believe it will not turn around.

JHEP01(2014)032

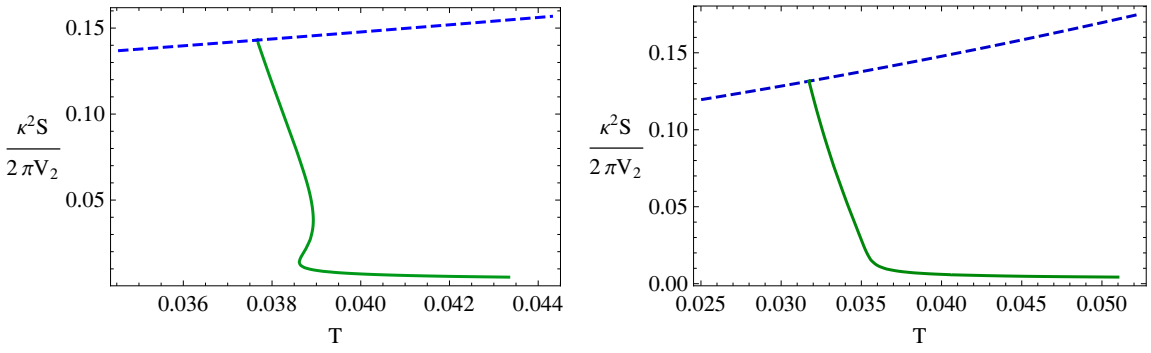

Figure 12. The thermal entropy S as a function of temperature for $q = 19/20$ (left) and $q = 9/10$ (right). The dashed blue curves come from the normal phase, while the solid curves from the condensed phase.

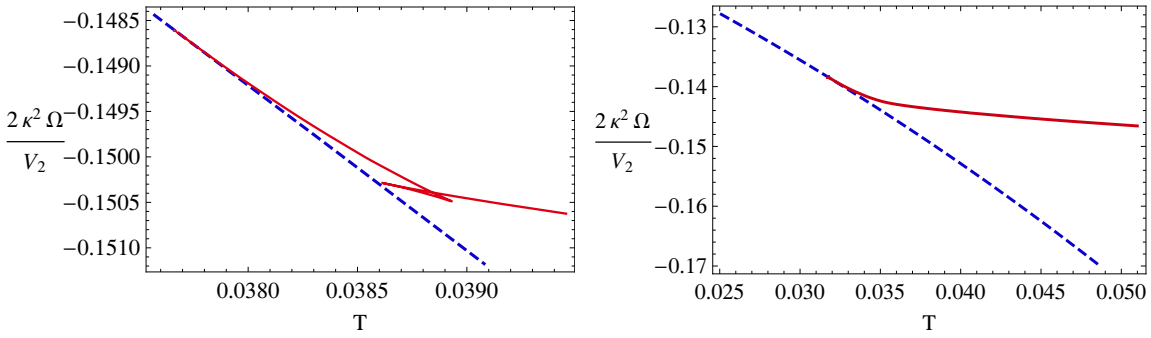

Figure 13. The free energy Ω as a function of temperature for $q = 19/20$ (left) and $q = 9/10$ (right). The dashed blue curves come from the normal phase, while the solid red curves from the condensed phase. The free energy of the condensed phase in the left plot forms a typical swallow tail. In both plots, the condensed phase has the free energy larger than the normal phase, and thus is not thermodynamically preferred.

configuration should have free energy less than the AdS Reissner-Nordström black hole describing the normalphase. Comparing Ω between the condensed phase and normal phase, we can clearly see in figure 13 that the condensed phase has free energy much larger than the normal phase and thus is not thermodynamically favored. Therefore these hairy black holes represent unstable branches that do not contribute to the thermodynamics. Similar phenomenon was previously found in ref. [31] through a phenomenological model, known as "exotic hairy black holes". Such a phenomenon also exists in some consistent truncations of string/M-theory in refs. [32, 33] as well as inhomogeneous black hole solutions in AdS space dual to spatially modulated phase of a field theory at finite chemical potential [34]. This phenomenon of a thermodynamically subdominant condensate at higher temperature is known as "retrograde condensation".[4]

[4]The terminology "retrograde condensation" was first introduced to describe the behavior of a binary mixture during isothermal compression above the critical temperature of the mixture [35]. A subdominant condensate can exist in this system in some temperature range.

JHEP01(2014)032

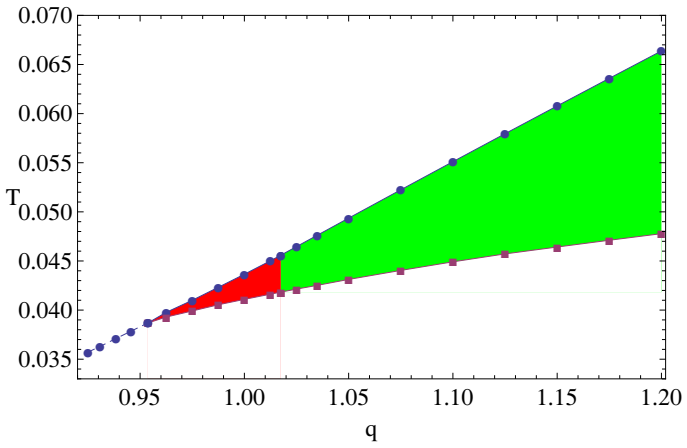

Figure 14. The (T, q) phase diagram for $m^2 = -3/16$. The green region is related to the condensed phase through a second order transition from the normal phase, while the red region is associated with the case by a first order transition. For other areas, the normal phase is thermodynamically favored. The transition temperature T_n for the retrograde condensation is denoted by the dashed line in the left down corner.

We summarize the main results of this subsection by constructing the (T, q) phase diagram in figure 14. The upper solid curve indicates the transition from the normal phase to the condensed phase as we lower the temperature, which is the combination of T_2 for $q > q_\alpha$ and T_1 for $q_\beta < q < q_\alpha$. The lower solid curve represents the minimal temperature T_0 at which hairy solutions terminate. The region between the two boundary curves shrinks as one increases the strength of the back reaction and the two curves intersect at q_β. The dashed curve for $q < q_\beta$ gives the value of T_n, above which a thermodynamically subdominant condensed phase appears.

We now return to the critical mass m_c^2. For very small m^2, we can find the temperature T_0 easily by directly numerical calculation. Figure 15 presents the temperature T_0 for each m^2. We find that the value of T_0 decreases quickly as one increases m^2 from its lower bound. But, to search for T_0 numerically becomes more and more difficult as the value of m^2 is close to the critical one. Due to the lake of numerical control at sufficiently low temperatures, we are not able to give the values of physical quantities, such as condensate $\langle \hat{J}_x \rangle$, charge density ρ and entropy S, at very low T. Nevertheless, believing T_0 as a function of m^2 exhibits a well-behaved behavior and using the extrapolation, we find that the value of m_c^2 locates at $m_c^2 = 0$ up to a numerical error.[5] There are also two other hints that support our numerical result for the value of m_c^2: (1) comparing our model to the SU(2) p-wave model, the effective mass of the vector operator is equal to zero for the latter, we find that the reduced equations of motion look very similar with each other and the asymptotical expansions near the boundary are the same. Since there does not exist any particular temperature at which the condensate terminates and turns around to high temperatures

[5]In the case with $m^2 = -399/160000$ and $q = 2$, we find the turning point is $T_0 \simeq 0.00429\mu$. For the case with $m^2 = 0$ and $q = 2$, we numerically solve the model up to the temperature $T \simeq 0.00038\mu$ with very high computational accuracy and find no turning point.

JHEP01(2014)032

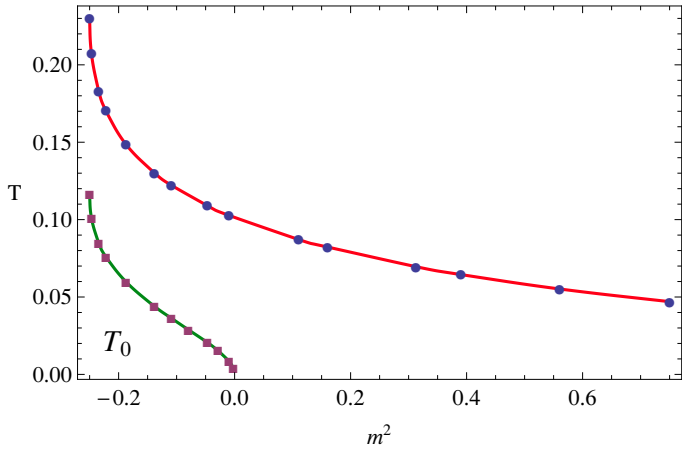

Figure 15. The transition temperature from the normal phase to the condensed phase (upper curve) and the turning temperature T_0 (lower curve) with respect to m^2. Here $q = 2$. The leftmost two points correspond to the mass square slightly above $m^2 = -1/4$.

in the SU(2) p-wave case, it is natural to expect that the result is also true in our model with $m^2 = 0$. Indeed, for the special case $m^2 = 0$, if we ignore the possible turning point T_0 at very low temperature, the model exhibits extremely similar behavior as the SU(2) p-wave model [22, 36]. Furthermore, our ongoing analysis of our model with the full back reaction in (4+1) dimensional black hole as well as soliton background cases exhibits all known phase structure presented in this paper. (2) Looking at the asymptotical expansion of ρ_x in (3.5), one can see that the leading term with coefficient ρ_{x-} for $m^2 > 0$ is divergent as $r \to \infty$. In this case such a term must be regarded as source term and set to be zero. In contrast, this term for $m^2 < 0$ is regular as $r \to \infty$. Similar to the case in the s-wave model [4], we may have freedom to consider ρ_{x-} either as source term or expectation value of the dual operator. The critical value of mass square is $m^2 = 0$. Thus, it is not surprised that the model exhibits distinguished behaviors for $m^2 < 0$ and $m^2 > 0$ numerically.

One may suspect that even for very large m^2 there exists a non zero but very small minimal temperature like T_0. Indeed, we can not rule out this possibility by numerical approach only. Nonetheless, for large $m^2 > m_c^2$, our numerical calculation indicates that the physical branch of $\langle \hat{J}_x \rangle$ (ρ and S) versus temperature may behave well up to zero temperature. In particular, we do not find any evidence of the branch turning back to a one at higher temperature as a characteristic of a zeroth order transition shown, for example, in figure 6.[6] Of course it is helpful to clear up this issue by constructing the extremal limit of the hairy black hole solutions. We leave this for future investigation.

We draw the plot of the critical temperature versus the mass of the vector field from the normal phase to the condensed phase in figure 15. One can see that the critical temperature decreases with the mass of ρ_μ at a given q. This behavior is also observed in holographic models involving a charged scalar field [37, 38].

[6] As a typical example, we choose the model parameters $m^2 = 3/4$ and $q = 43/40$. We manage to solve the coupled equations of motion (3.4) up to the temperature as low as $T \simeq 3.332 \times 10^{-6}\mu$ and find no evidence of the condensate turning around to a branch extending to the high temperature region.

JHEP01(2014)032

We did not find any hint in the probe limit that the condensate as well as other quantities turns back to a branch extending to the high temperature region at a certain temperature like T_0 [17]. Therefore, the appearance of T_0 is the consequence of the back reaction. For sufficiently large q, the back reaction can be ignored and we should recover the results in the probe limit. In other words, T_0 should be zero and the critical temperatures T_c and T_2 should arrive at some finite constants as $q \to \infty$. However, one can see from figure 14 that the value of T_0 increases with q, and from figure 5 and figure 14 that the critical temperatures T_c and T_2 from the normal phase to the condensed phase also increase with large q linearly. This is seemingly inconsistent with the expectation in the probe limit. In fact our numerical results are consistent with the probe limit. The reason is as follows. Note that the probe limit demands that one takes the limit $q \to \infty$, while keeping $q\rho_\mu$ and qA_μ fixed in our model. To compare our results to the ones in the probe limit, we should make the scaling transformation $\rho_\mu \to q\rho_\mu$ and $A_\mu \to qA_\mu$. Under such a transformation, the chemical potential μ becomes $q\mu$ and the temperature T changes to T/q. Therefore, it is the value T/q that corresponds to the temperature in the probe limit. Indeed, in our numerical calculations, we checked that $T_0/q \to 0$ and the critical temperatures T_c/q and T_2/q approach to some constants as $q \to \infty$. Therefore our numerical results are in agreement with the probe limit analysis.

Furthermore, we know from from (4.5) that to see whether the dual stress-energy tensor is isotropic or not, we have to extract the value of h_3 carefully in our calculations. We find that the numerical solutions presented in our paper have $h_3 = 0$ up to a numerical error ($\sim 10^{-14}$). It means that although the model has an anisotropic structure associated with the p-wave order with non-vanishing $\langle \hat{J}_x \rangle$ in the condensed phase, the stress-energy tensor is isotropic. This is the same as in the SU(2) p-wave model case[7] and is consistent with the arguments presented in ref. [39].

6 Conclusion and discussions

In this paper we studied a holographic p-wave superconductor model in a four dimensional Einstein-Maxwell-complex vector field theory with a negative cosmological constant. The complex vector field ρ_μ is charged under the Maxwell field. Taking the back reaction of matter fields into consideration, we managed to construct hairy black hole solutions which satisfy all asymptotic conditions. We found the model presents a rich phase structure controlled by the mass m and charge q of the vector field ρ_μ. We investigated possible phase transitions in detail. It turns out that there exist zeroth order, first order and second order phase transitions in this model. Hairy black holes were also found in the unusual higher temperature range $T > T_n$, which always have free energy higher than the normal phase. The phase diagrams in terms of the temperature and charge were constructed.

Our numerical calculation suggests the existence of a critical m^2 denoted as $m_c^2 = 0$. When $m^2 > m_c^2$, we have a second order phase transition from the normal phase to the

[7] The anisotropy of the stress-energy tensor in the SU(2) model is controlled by the constant f_2^b appearing in equation (21) of ref. [22]. It has been confirmed that the value of f_2^b should be vanishing up to a reasonable numerical error [39].

JHEP01(2014)032

condensed phase for the weak back reaction case. This transition becomes a first order one as we increase the strength of the back reaction. The transition temperature T_c decreases as we decrease the value of q, which means that the increase of the back reaction makes the transition more difficult. When $m^2 < m_c^2$, the thermodynamic behavior of the system changes a lot. Starting from the high temperature region, one can find the following transitions: for $q > q_\alpha$, the system undergoes a second order phase transition from the normal phase to the condensed phase at T_2 and as the temperature decreases to T_0, there is a zeroth order transition back to the normal phase; for $q_\beta < q < q_\alpha$, the system first undergoes a first order phase transition from the normal phase to the condensed phase at T_1, then at the lower temperature T_0, it comes back to the normal phase by a zeroth order transition; for $q < q_\beta$, we can only get hairy black hole solutions that are always subdominant in the free energy referred to as "retrograde condensation". Here the concrete values of q_α and q_β depend on the mass squared m^2 of the vector field ρ_μ.

It was argued in ref. [40] that the holographic free energy can be thought of as a sort of generalized version of Landau-Ginzburg free energy. In Landau-Ginzburg theory, it is usually assumed that the quadratic term depends on the temperature linearly while the fourth order term is not strongly temperature dependent. In our present study, we found the behaviors deviating from the mean field theory. In the context of Landau-Ginzburg theory, such deviation would be a sign of an unusual temperature dependence of the higher order terms. It should be stressed that our model is dual to a strongly coupled system. A priori the dual system does not obey the usual assumption for the free energy. It is in principle possible that there is some new temperature scale at which the coefficients of higher order terms change their signs, giving rise to non-standard phase transitions in the framework of Landau-Ginzburg theory.

Our study can be straightforwardly generalized to the higher dimensional case and other gravitational backgrounds, such as the AdS soliton backgrounds which can mimic the superconductor/insulator phase transition [41]. In a recent paper [42], we studied the effect of an applied magnetic field effect on the AdS soliton background, and found that the magnetic field can induce the AdS soliton instability due to the non-minimal coupling of the vector field and the background magnetic field. By comparing our complex vector field model to the SU(2) p-wave model with a constant non-Abelian magnetic field, we found that the SU(2) p-wave model can be recovered by the restriction $m^2 = 0$ and $\gamma = 1$ in our model with the ansatz in ref. [42]. It suggests that in some sense, the charged vector model is a generalization of the SU(2) p-wave model to the case with a general mass squared m^2 and gyromagnetic ratio γ for the vector field. Due to the adjustable parameter m, we can see in this paper that our model shows a much richer phase structure than the SU(2) p-wave model, thus can be used to describe more phenomena in dual strongly coupled systems.

In the present paper, we limited ourselves to a simple case with ρ_x non-vanishing only. In principle, in order to understand the full phase structure of the model at fixed chemical potential, one should search for the dominant thermodynamic configuration not only in this given sector but in a more general setup, especially turning on the temporal component of the charged vector ρ_t. This would of course be much more involved, since one should

JHEP01(2014)032

search for the hairy black hole configuration with the least free energy among all possible configurations. We will leave this issue for further study.

As a phenomenological approach, we consider the model as a p-wave superconducting (superfluid) one. Indeed, this toy model could be applicable in a wide variety of condensed matter systems and beyond. Indeed, as we have discussed in ref. [17], it may also be revelent for holographically mimicking the phenomenon that the QCD vacuum undergoes a phase transition to an exotic phase with charged ρ-meson condensed in a sufficiently strong magnetic field [43, 44].

As we have mentioned above, according to the symmetry of the macroscopic wave function or condensate of Cooper pairs in the real superconducting materials, the superconductor can be classified by s-wave, p-wave, d-wave and so on. The holographic s-wave model has well studied (especially with back reaction) in the literature. Adopting the present p-wave model, it is quite interesting to study holographic models with multiple superconducting order parameters, including the competition or coexistence between s-wave order and p-wave order or between two p-wave orders.[8] We will leave all these issues for further study.

Finally we like to mention that with suitable parameters m and q, our model shows the normal/superconducting/normal phase transition (see figure 14) as one lowers the temperature continuously. Such a phase transition is called reentrant phase transition in the literature [47]. The reentrant phase transition usually happens in the binary and multicomponent liquid mixtures. But it is interesting to note that such a phase transition also appears in some superconducting materials, for example, granular $BaPb_{0.75}Bi_{0.25}O_3$ compound [48] and cuprate superconductors [49]. Thus it would be of some interest to see whether our model is relevant to these superconducting phase transitions.

Acknowledgments

This work was supported in part by the National Natural Science Foundation of China (No. 10821504, No. 11035008, No. 11205226, No. 11305235, and No. 11375247), and in part by the Ministry of Science and Technology of China under Grant No. 2010CB833004.

[8] It might be difficult to combine the s-wave model [4] and the SU(2) p-wave model [9] in one theory, since the order parameter in the SU(2) model is charged under a U(1) subgroup of the Yang-Mills field and this U(1) subgroup can not play the role of the gauge group for the s-wave model in a natural manner. The current p-wave model is charged under a U(1) gauge group which also can be naturally taken as the gauge group of the s-wave order. The competition and coexistence between two s-wave orders were first studied in ref. [45] in the probe limit, and in ref. [18] with back reaction. More recently, ref. [46] constructed a model with a scalar triplet charged under a SU(2) gauge field, there the s-wave order and p-wave order can coexist.

JHEP01(2014)032

References

[1] J.M. Maldacena, *The large-N limit of superconformal field theories and supergravity*, *Adv. Theor. Math. Phys.* **2** (1998) 231 [*Int. J. Theor. Phys.* **38** (1999) 1113] [hep-th/9711200] [INSPIRE].

[2] S.S. Gubser, I.R. Klebanov and A.M. Polyakov, *Gauge theory correlators from noncritical string theory*, *Phys. Lett.* **B 428** (1998) 105 [hep-th/9802109] [INSPIRE].

[3] E. Witten, *Anti-de Sitter space and holography*, *Adv. Theor. Math. Phys.* **2** (1998) 253 [hep-th/9802150] [INSPIRE].

[4] S.A. Hartnoll, C.P. Herzog and G.T. Horowitz, *Building a holographic superconductor*, *Phys. Rev. Lett.* **101** (2008) 031601 [arXiv:0803.3295] [INSPIRE].

[5] S.A. Hartnoll, C.P. Herzog and G.T. Horowitz, *Holographic superconductors*, *JHEP* **12** (2008) 015 [arXiv:0810.1563] [INSPIRE].

[6] J.-W. Chen, Y.-J. Kao, D. Maity, W.-Y. Wen and C.-P. Yeh, *Towards a holographic model of d-wave superconductors*, *Phys. Rev.* **D 81** (2010) 106008 [arXiv:1003.2991] [INSPIRE].

[7] F. Benini, C.P. Herzog, R. Rahman and A. Yarom, *Gauge gravity duality for d-wave superconductors: prospects and challenges*, *JHEP* **11** (2010) 137 [arXiv:1007.1981] [INSPIRE].

[8] K.-Y. Kim and M. Taylor, *Holographic d-wave superconductors*, *JHEP* **08** (2013) 112 [arXiv:1304.6729] [INSPIRE].

[9] S.S. Gubser and S.S. Pufu, *The gravity dual of a p-wave superconductor*, *JHEP* **11** (2008) 033 [arXiv:0805.2960] [INSPIRE].

[10] M.M. Roberts and S.A. Hartnoll, *Pseudogap and time reversal breaking in a holographic superconductor*, *JHEP* **08** (2008) 035 [arXiv:0805.3898] [INSPIRE].

[11] H.-B. Zeng, W.-M. Sun and H.-S. Zong, *Supercurrent in p-wave holographic superconductor*, *Phys. Rev.* **D 83** (2011) 046010 [arXiv:1010.5039] [INSPIRE].

[12] R.-G. Cai, Z.-Y. Nie and H.-Q. Zhang, *Holographic phase transitions of p-wave superconductors in Gauss-Bonnet gravity with back-reaction*, *Phys. Rev.* **D 83** (2011) 066013 [arXiv:1012.5559] [INSPIRE].

[13] L.A. Pando Zayas and D. Reichmann, *A holographic chiral $p_x + ip_y$ superconductor*, *Phys. Rev.* **D 85** (2012) 106012 [arXiv:1108.4022] [INSPIRE].

[14] D. Momeni, N. Majd and R. Myrzakulov, *p-wave holographic superconductors with Weyl corrections*, *Europhys. Lett.* **97** (2012) 61001 [arXiv:1204.1246] [INSPIRE].

[15] D. Roychowdhury, *Holographic droplets in p-wave insulator/superconductor transition*, *JHEP* **05** (2013) 162 [arXiv:1304.6171] [INSPIRE].

[16] F. Aprile, D. Rodriguez-Gomez and J.G. Russo, *p-wave holographic superconductors and five-dimensional gauged supergravity*, *JHEP* **01** (2011) 056 [arXiv:1011.2172] [INSPIRE].

[17] R.-G. Cai, S. He, L. Li and L.-F. Li, *A holographic study on vector condensate induced by a magnetic field*, *JHEP* **12** (2013) 036 [arXiv:1309.2098] [INSPIRE].

[18] R.-G. Cai, L. Li, L.-F. Li and Y.-Q. Wang, *Competition and coexistence of order parameters in holographic multi-band superconductors*, *JHEP* **09** (2013) 074 [arXiv:1307.2768] [INSPIRE].

JHEP01(2014)032

[19] Y. Liu, K. Schalm, Y.-W. Sun and J. Zaanen, *Bose-Fermi competition in holographic metals*, *JHEP* **10** (2013) 064 [arXiv:1307.4572] [INSPIRE].

[20] F. Nitti, G. Policastro and T. Vanel, *Dressing the electron star in a holographic superconductor*, *JHEP* **10** (2013) 019 [arXiv:1307.4558] [INSPIRE].

[21] G.T. Horowitz and B. Way, *Complete phase diagrams for a holographic superconductor/insulator system*, *JHEP* **11** (2010) 011 [arXiv:1007.3714] [INSPIRE].

[22] M. Ammon, J. Erdmenger, V. Grass, P. Kerner and A. O'Bannon, *On holographic p-wave superfluids with back-reaction*, *Phys. Lett.* **B 686** (2010) 192 [arXiv:0912.3515] [INSPIRE].

[23] Y. Peng, Q. Pan and B. Wang, *Various types of phase transitions in the AdS soliton background*, *Phys. Lett.* **B 699** (2011) 383 [arXiv:1104.2478] [INSPIRE].

[24] R.-G. Cai, S. He, L. Li and L.-F. Li, *Entanglement entropy and Wilson loop in Stückelberg holographic insulator/superconductor model*, *JHEP* **10** (2012) 107 [arXiv:1209.1019] [INSPIRE].

[25] R.-G. Cai, L. Li, L.-F. Li and R.-K. Su, *Entanglement entropy in holographic p-wave superconductor/insulator model*, *JHEP* **06** (2013) 063 [arXiv:1303.4828] [INSPIRE].

[26] G.T. Horowitz and M.M. Roberts, *Holographic superconductors with various condensates*, *Phys. Rev.* **D 78** (2008) 126008 [arXiv:0810.1077] [INSPIRE].

[27] V. Balasubramanian and P. Kraus, *A stress tensor for anti-de Sitter gravity*, *Commun. Math. Phys.* **208** (1999) 413 [hep-th/9902121] [INSPIRE].

[28] S.S. Gubser, S.S. Pufu and F.D. Rocha, *Quantum critical superconductors in string theory and M-theory*, *Phys. Lett.* **B 683** (2010) 201 [arXiv:0908.0011] [INSPIRE].

[29] G.T. Horowitz and M.M. Roberts, *Zero temperature limit of holographic superconductors*, *JHEP* **11** (2009) 015 [arXiv:0908.3677] [INSPIRE].

[30] V.P. Maslov, *Zeroth-order phase transitions*, *Math. Notes* **76** (2004) 697.

[31] A. Buchel and C. Pagnutti, *Exotic hairy black holes*, *Nucl. Phys.* **B 824** (2010) 85 [arXiv:0904.1716] [INSPIRE].

[32] A. Donos and J.P. Gauntlett, *Superfluid black branes in $AdS_4 \times S^7$*, *JHEP* **06** (2011) 053 [arXiv:1104.4478] [INSPIRE].

[33] F. Aprile, D. Roest and J.G. Russo, *Holographic superconductors from gauged supergravity*, *JHEP* **06** (2011) 040 [arXiv:1104.4473] [INSPIRE].

[34] B. Withers, *Black branes dual to striped phases*, *Class. Quant. Grav.* **30** (2013) 155025 [arXiv:1304.0129] [INSPIRE].

[35] J.P. Kuenen, *Measurements on the surface of van der Waals for mixtures of carbonic acid and methyl chloride*, *Commun. Phys. Lab. Univ. Leiden* **4** (1892).

[36] A. Akhavan and M. Alishahiha, *p-wave holographic insulator/superconductor phase transition*, *Phys. Rev.* **D 83** (2011) 086003 [arXiv:1011.6158] [INSPIRE].

[37] F. Denef and S.A. Hartnoll, *Landscape of superconducting membranes*, *Phys. Rev.* **D 79** (2009) 126008 [arXiv:0901.1160] [INSPIRE].

[38] S.S. Gubser, C.P. Herzog, S.S. Pufu and T. Tesileanu, *Superconductors from superstrings*, *Phys. Rev. Lett.* **103** (2009) 141601 [arXiv:0907.3510] [INSPIRE].

JHEP01(2014)032

[39] A. Donos and J.P. Gauntlett, *On the thermodynamics of periodic AdS black branes*, *JHEP* **10** (2013) 038 [arXiv:1306.4937] [INSPIRE].

[40] F. Aprile, S. Franco, D. Rodriguez-Gomez and J.G. Russo, *Phenomenological models of holographic superconductors and Hall currents*, *JHEP* **05** (2010) 102 [arXiv:1003.4487] [INSPIRE].

[41] T. Nishioka, S. Ryu and T. Takayanagi, *Holographic superconductor/insulator transition at zero temperature*, *JHEP* **03** (2010) 131 [arXiv:0911.0962] [INSPIRE].

[42] R.-G. Cai, L. Li, L.-F. Li and Y. Wu, *Vector condensate and AdS soliton instability induced by a magnetic field*, arXiv:1311.7578 [INSPIRE].

[43] M.N. Chernodub, *Superconductivity of QCD vacuum in strong magnetic field*, *Phys. Rev.* **D 82** (2010) 085011 [arXiv:1008.1055] [INSPIRE].

[44] M.N. Chernodub, *Spontaneous electromagnetic superconductivity of vacuum in strong magnetic field: evidence from the Nambu-Jona-Lasinio model*, *Phys. Rev. Lett.* **106** (2011) 142003 [arXiv:1101.0117] [INSPIRE].

[45] P. Basu, J. He, A. Mukherjee, M. Rozali and H.-H. Shieh, *Competing holographic orders*, *JHEP* **10** (2010) 092 [arXiv:1007.3480] [INSPIRE].

[46] Z.-Y. Nie, R.-G. Cai, X. Gao and H. Zeng, *Competition between the s-wave and p-wave superconductivity phases in a holographic model*, *JHEP* **11** (2013) 087 [arXiv:1309.2204] [INSPIRE].

[47] T. Narayanan and A. Kumar, *Reentrant phase transitions in multicomponent liquid mixtures*, *Phys. Rept.* **249** (1994) 135.

[48] T.H. Lin et al., *Observation of a reentrant superconducting resistive transition in granular* $BaPb_{0.75}Bi_{0.25}O_3$ *superconductor*, *Phys. Rev.* **B 29** (1984) 1493.

[49] Y. Zhao et al., *Normal-state reentrant behavior in superconducting* $Bi_2Sr_2CaCu_2O_8/Bi_2Sr_2Ca_2Cu_3O_{10}$ *intergrowth single crystals*, *Phys. Rev.* **B 51** (1995) 3134.

JHEP01(2014)032